Microscopic Theory of Exciton Annihilation: Application to the LH2 Antenna System

Ben Brüggemann,*,† Jennifer L. Herek,‡ Villy Sundström,‡ Tõnu Pullerits,‡ and Volkhard May†

Institute of Physics, Humboldt-University at Berlin, Hausvogteiplatz 5−7, 10117 Berlin, Germany, and Department of Chemical Physics, Chemical Center, Lund University, P.O. Box 124, 221 00 Lund, Sweden

Received: May 31, 2001; In Final Form: August 6, 2001

The multiexciton density matrix theory is utilized to achieve a microscopic description of exciton−exciton annihilation (EEA). We apply the theory to the 18 bacteriochlorophyll (BChl) molecules of the B850 ring of the light-harvesting complex LH2 of *Rhodobacter sphaeroides.* The simulation of the EEA process reproduces the intensity-dependent transient absorption kinetic experiments very well, and insight is obtained on microscopic parameters such as the internal conversion rate of BChl in LH2. The exciton dynamics and the different relaxation processes are visualized by constructing a multiexciton spectrogram.

Introduction

Femtosecond spectroscopy has been used to reveal details of excitation energy (exciton) relaxation and transfer in various types of chromophore complexes. To study higher excited states and to discover new relaxation channels such as exciton−exciton annihilation (EEA), it is a common practice to vary the intensity of the laser pulse used to excite the chromophore complex. Annihilation experiments have been reported for dye aggregates[1,2] and various photosynthetic antenna systems: the FMO-complex,[3] LH1,[4,5] and LH2.[6] So far, EEA has been often described by the rate equation $\partial n(\mathbf{r},t)/\partial t = -\gamma n(\mathbf{r},t)^2$ with the exciton density $n(\mathbf{r},t)$ at the spatial position $\mathbf{r}$ and the annihilation rate constant γ (for a recent overview, see ref 7). Besides such a macroscopic description valid for larger aggregates, various microscopic theories have been presented including a correct computation of the rate constant γ.[8−11] An anharmonic oscillator description of Frenkel excitons could be utilized recently, too.[12] In this letter, we report on the description of EEA processes by a generalization of the multiexciton density matrix theory, i.e., the approach which directly accounts for multiple electronic excitations in chromophore complexes.[13] The theory is applied to the B850 ring of the LH2 complex of *Rhodobacter sphaeroides* with 18 bacteriochlorophylls (BChls) (see, for example, ref 15).

EEA is usally described as follows. If two excitations being in the S_1-state of the chromophores move close together, their excitation energy can be used to create a higher excited S_n-state ($n > 1$) at one chromophore leaving behind the other in the S_0 ground state (exciton fusion). In a second step, an ultrafast internal conversion process moves the chromophore that is just in the higher excited S_n-state back to the S_1-state. If this view on EEA is embedded into the multiexciton theory, the description automatically accounts for the exciton fusion because the two-exciton states incorporate the mixture of two S_1-excitations and a single S_n-excitation. Now, EEA is obtained as an effective radiationless transition from the two-exciton to the single-exciton manifold[12] (for details, see also ref 14). After this has been included into the density matrix theory, we calculate the transient absorption spectra of ref 16, and the results of our simulations are visualized with the help of a multiexciton spectrogram. Details of the measurements are not reported here but can be found in ref 16.

Multiexciton Density Matrix Approach

Besides the ground-state and the single-exciton state, the multiexciton theory includes multiple excitations, i.e., the simultanous presence of two, three, etc. excitons, with the specification that higher excited states (S_n-states) of single chromophores are accounted for, too. The two-exciton states, for example, include states in which the excitations are on separated chromophores as well as states in which an individual chromophore is in the S_n-state. Taking the complete Hamiltonian which includes electronic chromophore excitations and an electronic interchromophore coupling (dipole−dipole interaction), its diagonalization yields the multiexciton states, $|\alpha_N\rangle$, corresponding to the presence of N-fold excitations in the complex. Once these states have been used as a representation of the density operator, we end up with the multiexciton density matrix $\rho(\alpha_N,\beta_M;t)$. If $\alpha_N = \beta_N$, it describes the multiexciton population in the N-exciton manifold, otherwise the density matrix elements represent so-called coherences (within the same manifold as well as between different ones).

The equation of motion for $\rho(\alpha_N,\beta_M;t)$ has to account for electronic excitation energy dissipation as well as a coupling to the radiation field. It has been derived previously in the usual Markov and Bloch approximation[13,17] and reads

$$\frac{\partial}{\partial t}\rho(\alpha_N,\beta_M;t) = -i\Omega(\alpha_N,\beta_M)\rho(\alpha_N,\beta_M;t) + \left(\frac{\partial}{\partial t}\rho(\alpha_N,\beta_M;t)\right)_{\text{diss}} + \left(\frac{\partial}{\partial t}\rho(\alpha_N,\beta_M;t)\right)_{\text{field}} \quad (1)$$

where $\hbar\Omega(\alpha_N,\beta_M)$ is the energy difference of the two states, α_N and β_M. The dissipative part includes both the inter- and intramanifold relaxation:

* To whom correspondence should be addressed. E-mail: ben.brueggemann@physik.hu-berlin.de.
† Humboldt-University at Berlin.
‡ Chemical Center, Lund University.

10.1021/jp012072y CCC: $20.00
Published on Web 10/31/2001

$$\left(\frac{\partial}{\partial t}\rho(\alpha_N,\beta_M;t)\right)_{\text{diss}} = -\delta_{\alpha_N\beta_M}\Big(\sum_{\gamma_N} k(\alpha_N,\gamma_N)\rho(\alpha_N,\alpha_N;t) - \sum_{\gamma_N} k(\gamma_N,\alpha_N)\rho(\gamma_N,\gamma_N;t) + \sum_{\gamma_{N-1}} k(\alpha_N,\gamma_{N-1})\rho(\alpha_N,\alpha_N;t) - \sum_{\gamma_{N+1}} k(\gamma_{N+1},\alpha_N)\rho(\gamma_{N+1},\gamma_{N+1};t)\Big) - (1-\delta_{\alpha_N\beta_M})(\Gamma(\alpha_N) + \Gamma(\beta_M))\rho(\alpha_N,\beta_M;t) \quad (2)$$

The field part accounts for optical transitions and is given by

$$\left(\frac{\partial}{\partial t}\rho(\alpha_N,\beta_M;t)\right)_{\text{field}} = \frac{i}{\hbar}\mathbf{E}(t)\Big(\sum_{\gamma_{N\pm1}} \mu(\alpha_N,\gamma_{N\pm1})\rho(\gamma_{N\pm1},\beta_M;t) - \sum_{\gamma_{M\pm1}} \rho(\alpha_N,\gamma_{M\pm1};t)\mu(\gamma_{M\pm1},\beta_M)\Big) \quad (3)$$

where $\mu(\alpha_N,\gamma_{N\pm1})$ denotes the transition dipole moment. The sum goes over the states of the neighbored manifolds γ_{N+1} and γ_{N-1} or γ_{M+1} and γ_{M-1}. In the dissipative part, the damping rates for the so-called coherences are

$$\Gamma(\alpha_N) = \frac{1}{2}\sum_{\beta_M} k(\alpha_N,\beta_M) \quad (4)$$

The intra manifold relaxation (i.e., $M = N$) is given by[13]

$$k(\alpha_N,\beta_N) = 2\pi\Omega^2(\alpha_N,\beta_N)[1 + n(\Omega(\alpha_N,\beta_N))]\theta(\alpha_N,\beta_N)[j(\Omega(\alpha_N,\beta_N)) - j(\Omega(\beta_N,\alpha_N))] \quad (5)$$

where $n(\omega)$ is the Bose−Einstein distribution, the $\theta(\alpha_N,\beta_N)$ comprise the multiexciton vibrational coupling constants, and $j(\omega)$ denotes a site-independent spectral density. We have taken a form for $j(\omega)$ which has been experimentally determined for the LH2 in ref 18. It accounts for the modulation of the chromophore excitation energies by vibrational modes, but for simplicity, we neglect the modulation of the dipole−dipole interaction. The second type of rate constants describes the intermanifold relaxation, i.e., the EEA process. If related to the transition between the two- and the one-exciton manifold, it reads

$$k(\alpha_2,\beta_1) = \sum_m |C_{\alpha_2}(m,S_n)|^2 |C_{\beta_1}(m,S_1)|^2 k_m^{(\text{IC})} \quad (6)$$

where $|C_{\alpha_2}(m,S_n)|^2$ is the probability that within the two-exciton state $|\alpha_2\rangle$ the mth chromophore is in the higher excited S_n-state. The mth chromophore relaxes via internal conversion from the S_n- to the S_1-state with the rate of $k_m^{(\text{IC})}$. With a probability of $|C_{\beta_1}(m,S_1)|^2$, the system finds itself afterward in the one-exciton state $|\beta_1\rangle$.

To reduce the computational costs, we want to get rid of the highly oscillatoric behavior of the elements of the multiexciton density matrix with different manifold indices. Therefore, we expand the reduced density matrix in plane waves of the mean intermanifold transition frequency $\bar{\omega}$

$$\rho(\alpha_N,\beta_M;t) = \sum_{n=-\infty}^{\infty} e^{in\bar{\omega}t}\rho^{(n)}(\alpha_N,\beta_M;t) \quad (7)$$

and express the electric field as $\mathbf{E}(t) = \sum_p \tilde{\mathbf{E}}_p(t)\cos(\omega_p t)$, where the frequencies are in the same range, $\omega_p \approx \bar{\omega}$. The summation of the electric field extends over both the excitation and probe pulses. Neglecting the fast oscillating parts, i.e., using the rotating wave approximation, and remembering that the dipole operator couples only between different manifolds, we obtain an expression in which the regions of the density matrix with different multiexciton indices were transformed with different frequencies. We still have only one density matrix and all frequencies of the order of $\bar{\omega}$ are eliminated, making numerical calculation easier.

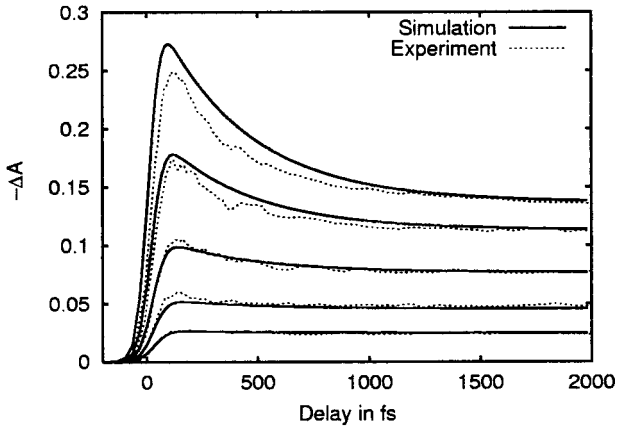

Figure 1. Transient absorption kinetics versus delay time for pump pulse with 100 fs duration and energies of 128, 64, 32, 16, and 8 μJ/cm^2 (from top to bottom). Pump pulse wavelength was 850 nm; probe pulse wavelength was 860 nm. Experimental (dotted) and simulated (solid) values are shown.

Numerical Results and Discussion

For the simulation of the spectra of the B850 ring of LH2, we have taken the dipole moments, coupling parameters, and energies as given in ref 15. The dipole moment of the $S_1 \rightarrow S_n$ transition of BChl is estimated to be of similar magnitude as the $S_0 \rightarrow S_1$ dipole moment;[19,20] therefore, we took the mean dipole−dipole coupling constant of the B850. It should be pointed out that beside the overall system bath coupling factor, which has been chosen to fit the long-time transient absorption signal, the only fitting parameter in our model, is the internal conversion rate, k_{IC}, of a single BChl.

The transient absorption was calculated by $\Delta A = (A(\omega_{\text{pu}},\omega_{\text{pr}}) - A(\omega_{\text{pr}}))/A(\omega_{\text{pr}})$, where $A(\omega_{\text{pu}},\omega_{\text{pr}})$ is the absorption of the probe pulse at the presence of the pump pulse and $A(\omega_{\text{pr}})$ is the absorption in the absence of the pump pulse. According to the experiment, we used in the simulations for both the pump and the probe pulse linearly polarized electric field-pulses of 100 fs duration with a Gaussian envelope and with the magic angle (54.7°) between the polarization directions. The orientational average has been considered in the simplest way by multiplying the transient absorption by a factor of $^1/_3$. We have taken a sum over four different phases between pump and probe pulse to extract the part of the absorption that is linear in the probe-pulse intensity.[21] The inclusion of static disorder has been left for further investigations.

To determine the internal conversion rate, we fitted the measured transient absorption decay at early times and for the highest excitation intensities. The respective time constant for internal conversion is 70 ± 5 fs. With this and the above-mentioned fixed parameters, the experimental transient absorption kinetics at different excitation intensities of the experiment could be simulated very well (Figure 1). In a recent article,[16] it was estimated that for the highest excitation intensities used here, the average number of excitations per LH2 is 2−3. This justifies the neglect of higher excited states beyond the two-exciton manifold, at least for the lower intensities. Nevertheless,

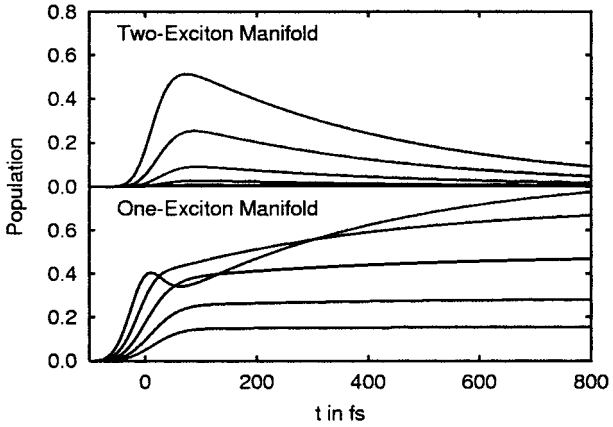

Figure 2. Population of the one- and two-exciton manifold for pump pulse energies as in Figure 1.

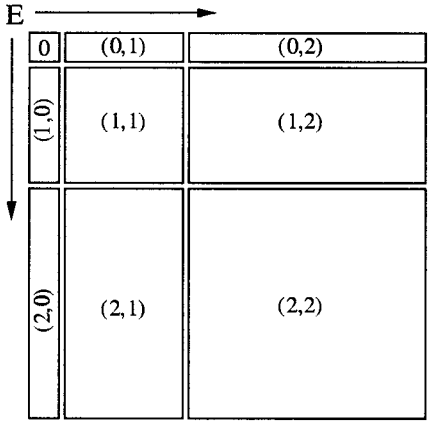

Figure 3. Scheme of the multiexciton spectrogram. The elements of the multiexciton density matrix are ordered by the corresponding eigenenergies, increasing from left to right and top to bottom. Parts with different manifold indices, $M, N = 0, 1, 2$, are separated as shown.

there is some deviation from the measured data at the two highest intensities, indicating that excited-state absorption from the two-exciton to the three-exciton state becomes important. (Its neglect leads to an overestimation of the signals.)

Figure 2 shows the overall populations, $P_M(t) = \sum_{\alpha_M} |\rho(\alpha_M,\alpha_M;t)|$ ($M = 0, 1, 2$) with $\sum_{M=0,1,2} P_M(t) = 1$ calculated for the different pump intensities of Figure 1. The population decay from the two-exciton manifold into the single-exciton manifold through the EEA process can be clearly identified. During the pump-pulse action, processes such as ground-state absorption ($0 \rightarrow 1$), excited-state absorption ($1 \rightarrow 2$), and stimulated emission ($2 \rightarrow 1$, $1 \rightarrow 0$) occur. At the highest pump intensity, there is a decrease in the one-exciton manifold at the end of the pump pulse, which is caused by a combination of ground-state depletion and excited-state absorption.[14]

Having fixed the parameters, one can visualize some otherwise unmeasurable internal dynamics of the system. In the multiexciton spectrogram, we plot the absolute value of each element of the multiexciton density matrix $|\rho(\alpha_N,\beta_N;t)|$ ordered by energy as shown in Figure 3 with a logarithmic color scale (Figure 4). The elements $|\rho(\alpha_N,\beta_M;t)|$ ($N = 0, 1, 2$) belonging to the same manifold represent populations (diagonal part, $\alpha_N = \beta_N$) and coherences (off-diagonal part) of the N-exciton states α_N and β_N. In contrast the elements $|\rho(\alpha_N,\beta_M;t)|$ with $N \neq M$ describe coherences between different manifolds caused by the coupling to the external field. The pictures provide the basis for a quantitative discussion of the main features of the dissipative dynamics. The pump pulse excites both populations

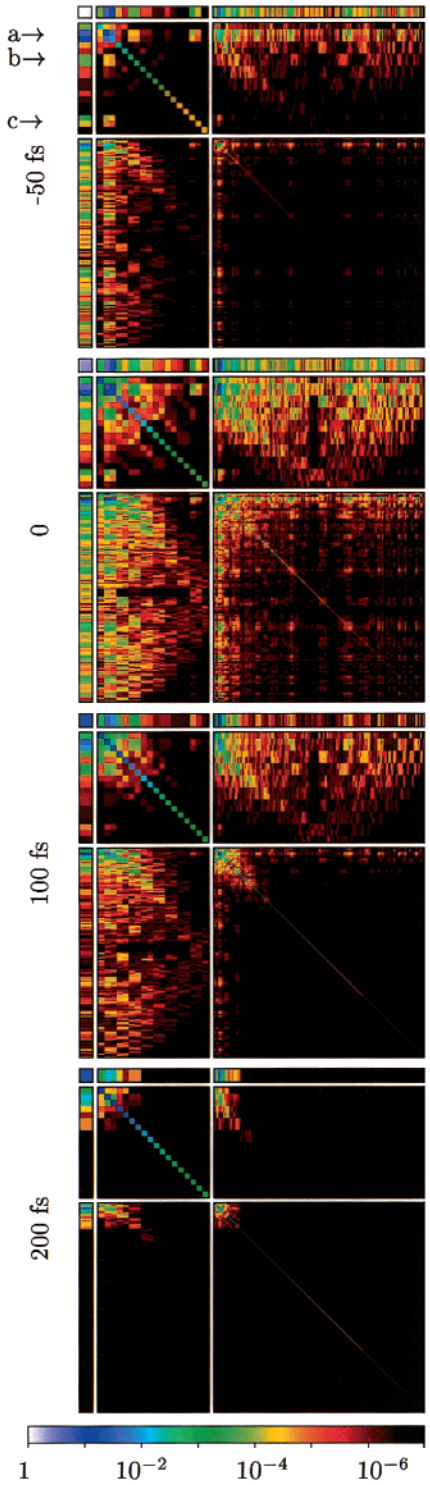

Figure 4. Multiexciton spectrogram for the highest pump intensity of Figure 1 at −50 fs, pump pulse maximum, and 100 and 200 fs delay time (from top to bottom). The absolute value of each density-matrix element, $|\rho(\alpha_N,\beta_M;t)|$, is shown by a logarithmic color scale. See also Figure 3. The coherences labeled a, b, and c are discussed in the text.

and coherences. Looking at the coherences between the ground and single-exciton state, one can distinguish between the two strongly allowed transitions (marked as "a" in Figure 4) and two weaker ones at higher energies (marked as "c" in Figure 4), which are well-known from other studies of the completely symmetric LH2.[15] The two transitions marked as "b" in Figure 4 are mediated by the two-exciton manifold, as could be clarified by a detailed inspection of the time evolution.[14] Between the

one-exciton and the two-exciton manifold, quite a number of transitions are allowed. Both the coherences and populations relax to the low-energy side of the corresponding manifold. After a while, the coherences die out, and the one-exciton population thermalizes.

In conclusion, we can state that our multiexciton density matrix not only allowed for a reproduction of measured data, and in this way for a determination of the BChl internal conversion rate, but also gave a detailed insight into the microscopic dynamics. Here, we concentrated on the energy representation of the internal multiexciton dynamics offering a direct access to the optical excitation and the different relaxation processes. The real-space representation of the multiexciton dynamics and thus of EEA will be discussed in detail in a forthcoming paper.

Acknowledgment. The cooperation of the group of V. May in Berlin with the group of V. Sundström in Lund has been supported by the ESF ULTRA program. Financial support by the Deutsche Forschungsgemeinschaft (Project Ma1356-7, B.B.) is gratefully acknowledged.

References and Notes

(1) Sundström, V.; Gillbro, T.; Gadonas, R. A.; Piskarskas, A. *J. Chem. Phys.* **1988**, *89*, 2754.
(2) Stiel, H.; Daehne, S.; Teuchner, K. *J. Lumin.* **1988**, *39*, 351.
(3) Gulbinas, V.; Valkunas, L.; Kuciauscas, D.; Katilius, E.; Liuolia, V.; Zhou, W.; Blankenship, R. E. *J. Phys. Chem.* **1996**, *100*, 17950.
(4) Bradforth, S. E.; Jimenez, R.; van Mourik, F.; van Grondelle, R.; Fleming, G. R. *J. Phys. Chem.* **1995**, *99*, 16179.
(5) Valkunas, L.; Akesson, E.; Pullerits, T.; Sundström, V. *Biophys. J.* **1996**, *70*, 2373.
(6) Ma, Y.-Z.; Cogdell, R. J.; Gillbro, T. *J. Phys. Chem B* **1997**, *101*, 1087.
(7) Van Amerongen, H.; Valkunas, L.; van Grondelle, R. *Photosynthetic Excitons*, 1st ed.; World Scientific: Singapore, 2000; Chapter 12.
(8) Suna, A. *Phys. Rev. B.* **1970**, *1*, 1716.
(9) Gaižauskas, E.; Feller, K.-H.; Gadonas, R. *Opt. Commun.* **1995**, *118*, 360.
(10) Malyshev, V. A.; Glaeske, H.; Feller, K.-H. *Chem. Phys. Lett.* **1999**, *305*, 117.
(11) Ryzhov, I. V.; Kozlov, G. G.; Malyshev, V. A.; Knoester, J. *J. Chem. Phys.* **2001**, *114*, 5322.
(12) Renger, T.; May, V.; Sundström, V.; Kühn, O. *J. Chin. Chem. Soc.* **2000**, *47*, 807.
(13) Renger, T.; May, V.; Kühn, O. *Phys. Rep.* **2001**, *343*, 137.
(14) Brüggemann, B.; May, V., to be submitted for publication.
(15) Sundström, V.; Pullerits, T.; van Grondelle, R. *J. Phys. Chem. B* **1999**, *103*, 2327.
(16) Trinkunas, G.; Herek, J. L.; Polívka, T.; Sundström, V.; Pullerits, T. *Phys. Rev. Lett.* **2001**, *86*, 4167.
(17) Renger, T.; May, V. *J. Phys. Chem. B* **1997**, *101*, 7232.
(18) Kühn, O.; Sundström, V.; Pullerits, T. *Chem. Phys.*, submitted for publication.
(19) Becker, M.; Nagarajan, V.; Parson, W. W. *J. Am. Chem. Soc.* **1991**, *113*, 6840.
(20) Martinsson, P.; Sundström, V.; Åkesson, E. *FEBS Lett.* **2000**, *465*, 107.
(21) Seidner, L.; Stock, G.; Domcke, W. *J. Chem. Phys* **1995**, *103*, 3998.